Supporting Information

Kwan *et al.* 10.1073/pnas.0805199105

SI Methods

Primary Culture Preparation. Hippocampal cultures were prepared as described in ref. 1 from hippocampi of embryonic day 18 Sprague–Dawley or Fischer 344 rats (BrainBits LLC). Tissues were dissociated with papain (Worthington Biochemicals) and mechanical trituration. The cultures were incubated in 5% CO_2 at 37°C, and half of the medium was exchanged every 4 days. The medium consisted of 2% B-27 supplement in phenol red-free Neurobasal medium with 1 mM GlutaMAX-1 (all from Invitrogen). Before imaging, the medium was replaced with a buffer solution containing 135 mM NaCl, 5 mM KCl, 1 mM $MgCl_2$, 1.8 mM $CaCl_2$, and 20 mM Hepes.

Nocodazole. For experiments with nocodazole, acute hippocampal slices were held under nylon grid anchors in an artificial cerebrospinal fluid (ACSF)-filled glass-bottom dish (World Precision Instruments). During treatment, nocodazole was dissolved in DMSO (1% of ACSF volume) and added to the dish, yielding a final concentration of 25 μM. Control slices were immersed in ACSF with only the DMSO solvent. The dish remained at room temperature and was bubbled continuously with 95% O_2 and 5% CO_2. Average second-harmonic generation (SHG) intensities were obtained from images obtained 10 min before and 40 min after drug application. Background estimated from adjacent empty regions was subtracted.

Numerical Simulation. The second-harmonic field $E_{2\omega}$ at a location (θ, φ, R) generated by dipoles lying parallel to the y axis is described (2, 3) by

$$E_{2\omega}(\theta, \varphi, R) \propto \beta \cdot E_\omega^2 \cdot \frac{\sin\psi\hat{\omega}}{R} \cdot \iiint dxdydz \cdot C(x,y,z) \cdot \exp(i \cdot 2 \cdot \zeta \cdot k_\omega \cdot z) \exp\left(\frac{-2(x^2+y^2)}{w^2} - \frac{2 \cdot z^2}{w_z^2}\right) \cdot \exp[-ik_{2\omega}(z\cos\theta + x\sin\varphi\sin\theta + y\cos\varphi\sin\theta)]$$

where β is the dipole hyperpolarizability, ψ is the angle subtended from the y axis, k is the wave vector, E_ω is the excitation field strength, w is the beam waist, ξ is the Gouy phase shift parameter, and $C(x,y,z)$ is the spatial concentration of the second-harmonic-generating dipoles. The term $C(x,y,z)$ can be either positive or negative, depending on the orientation of the dipoles. In this formalism, the microtubule arrays lie along the y axis, and the excitation propagates along the z axis. Forward-directed second-harmonic intensity, observable during most imaging experiments, would be proportional to the integral of $(E_{2\omega})^2$ from $\theta = 0$ to $\pi/2$. This is an approximation because objectives do not collect all forward-directed second-harmonic intensity. We have examined the far-field SHG intensity distribution [supporting information (SI) Fig. S2], which shows that most of the signal is emitted along the z axis and thus would be collected by objectives with relatively high numerical apertures.

To interpret the second-harmonic field, we note that intensity of the emitting field will depend on (*i*) the number of microtubules within the focal volume [reflected by the spatial integration of scatterer distribution $C(x,y,z)$ and beam intensity profile $\exp(-(x^2+y^2)/w^2 - 2^*z^2/w_z^2)$] and (*ii*) the spatial arrangement of the microtubules [reflected by the spatial integration of $C(x,y,z)$ and the Gouy phase anomaly $\exp(i^*2^*\xi^*k^*z)$], especially if the spatial length scale is comparable to the wavelength, as in the case for microtubule spacings in neurites. Furthermore, because the excitation field strength E_ω and the hyperpolarizability β appear only outside the integral, ratios of intensities $(E_{2\omega})^2$ would cancel these constants. This observation is useful for measurements because *in situ* determination of E_ω and β is difficult.

To estimate W_z and w, the excitation was approximated as a focused laser beam that has a Gaussian intensity profile and a Gouy phase shift across the focal plane (2). We use numerical values obtained by fits to exact field calculations (4). The numerical aperture of the excitation objective, 0.7, is used for calculating w.

To approximate $C(x,y,z)$, a microtubule array was defined as a hexagonal close-packed grid of microtubules, each modeled as a linear array of dipoles. The intermicrotubule spacing was 22 nm for axons and 64 nm for dendrites (5). The interdipole distance was 8 nm, the same as the longitudinal length of individual tubulin subunits. To verify that the result is insensitive to our structural assumptions, we performed simulations with shorter interdipole distances, with microtubule modeled as a ring of linear dipole arrays, analogous to protofilaments, and with arrays of square close-packed grid. These modifications yielded similar results so we opted for the simple geometry as described.

The calculation was implemented in MATLAB. We defined four classes of neurites: apical dendrites (spacing 64 nm, diameter 3 μm), basal dendrites (spacing 64 nm, diameter 1 μm), distal dendrites (spacing 64 nm, diameter 0.5 μm), and axons (spacing 22 nm, diameter 0.17 μm). The neurite diameters were obtained from literature (6, 7). In the case of apical dendrites, we confirmed the neurite diameter by measuring in the hippocampus and in the neocortex of adult *Thy1*-YFPH and obtained values of 2.7 ± 0.5 μm and 2.9 ± 0.4 μm, respectively. For each type of neurite, we simulated and calculated the second-harmonic intensity for a particular microtubule distribution. The distribution depends on the polarity, which the program used to set the orientation of each microtubule, plus-end or minus-end distal, probabilistically. We repeat the simulation 100 times for each neurite type at polarity intervals of 5%.

The numerical simulation assumes that plus- and minus-end distal microtubules are located randomly within the neurite. However, it is also possible that there may be a bias for the locations of microtubules depending on their polarity. For example, if all of the plus-end distal microtubules are located in the center of the neurite while the minus-end distal microtubules are in the periphery, then the calculated SHG intensities will be drastically different. So far, studies (5, 8) on the spatial organization of microtubules within neurites seem to suggest a hexagonally packed distribution with no strong bias on polarity, but this has not been verified in most types of neurons, especially from native tissues.

Error Analysis. We determine the uncertainties when estimating the microtubule polarity. There are two sources of uncertainties: forward/backward (f/b) SHG ratio measurement and numerical simulation. The uncertainty in the f/b SHG ratio measurement is estimated by the standard deviation of f/b SHG ratio (f/b ratio ± SD_{meas}) measured from >10 neurites across the field of view. The uncertainty in the numerical simulation (Sim ratio ±

SD_{Sim}) results from differing simulated f/b ratio in the various possible spatial distributions of microtubules. Both of these uncertainties are then propagated to estimate the error bounds of the polarity values by using Fig. 4*C*. We estimated that the upper error bound is the value when (Sim ratio − SD_{sim}) is equal to (f/b ratio + SD_{meas}). Similarly, the lower error bound is the value when (Sim ratio + SD_{sim}) is equal to (f/b ratio − SD_{meas}). Because of the nonlinear dependence of polarity on f/b SHG ratio, the error bounds are asymmetric.

1. Dombeck DA, *et al.* (2003) Uniform polarity microtubule assemblies imaged in native brain tissue by second-harmonic generation microscopy. *Proc Natl Acad Sci USA* 100:7081–7086.
2. Moreaux L, Sandre O, Mertz J (2000) Membrane imaging by second-harmonic generation microscopy. *J Opt Soc Am B* 17:1685–1694.
3. Williams RM, Zipfel WR, Webb WW (2005) Interpreting second-harmonic generation images of collagen I fibrils. *Biophys J* 88:1377–1386.
4. Zipfel WR, Williams RM, Webb WW (2003) Nonlinear magic: Multiphoton microscopy in the biosciences. *Nat Biotechnol* 21:1369–1377.
5. Chen J, Kanai Y, Cowan NJ, Hirokawa N (1992) Projection domains of MAP2 and tau determine spacings between microtubules in dendrites and axons. *Nature* 360:674–677.
6. Fiala JC, Harris KM (1999) *Dendrites*, eds Stuart G, Spruston N, Hausser M (Oxford Univ Press, New York), pp 1–34.
7. Shephard GM, Harris KM (1998) Three-dimensional structure and composition of CA3–CA1 axons in rat hippocampal slices: Implications for presynaptic connectivity and compartmentalization. *J Neurosci* 18:8300–8310.
8. Takahashi D, *et al.* (2007) Rearrangement of microtubule polarity orientation during conversion of dendrites to axons in cultured pyramidal neurons. *Cell Motil Cytoskel* 64:347–359.
9. Baas PW, Ahmad FJ, Pienkowski TP, Brown A, Black MM (1993) Sites of microtubule stabilization for the axon. *J Neurosci* 13:2177–2185.

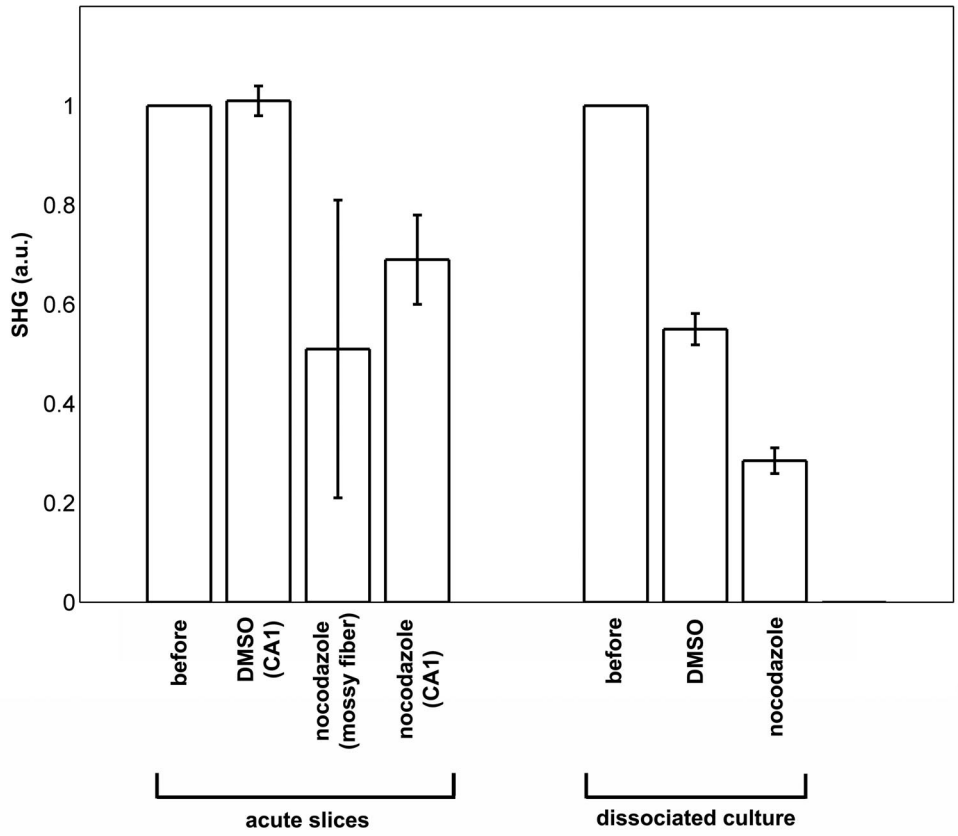

Fig. S1. Effect of nocodazole on SHG from acute slices and dissociated culture. Large losses in SHG imply that the observed signal originates from microtubules. The signal losses were partial in acute slices ($n = 2$ for each case), possibly because of insufficient penetration of nocodazole, but also could be because of stabilized microtubules in neurites, as described in ref. 9 in *SI Methods*. In cultures ($n = 4$), SHG loss was more pronounced, but DMSO also had an adverse effect. The experiment was performed at room temperature as described in *SI Methods*.

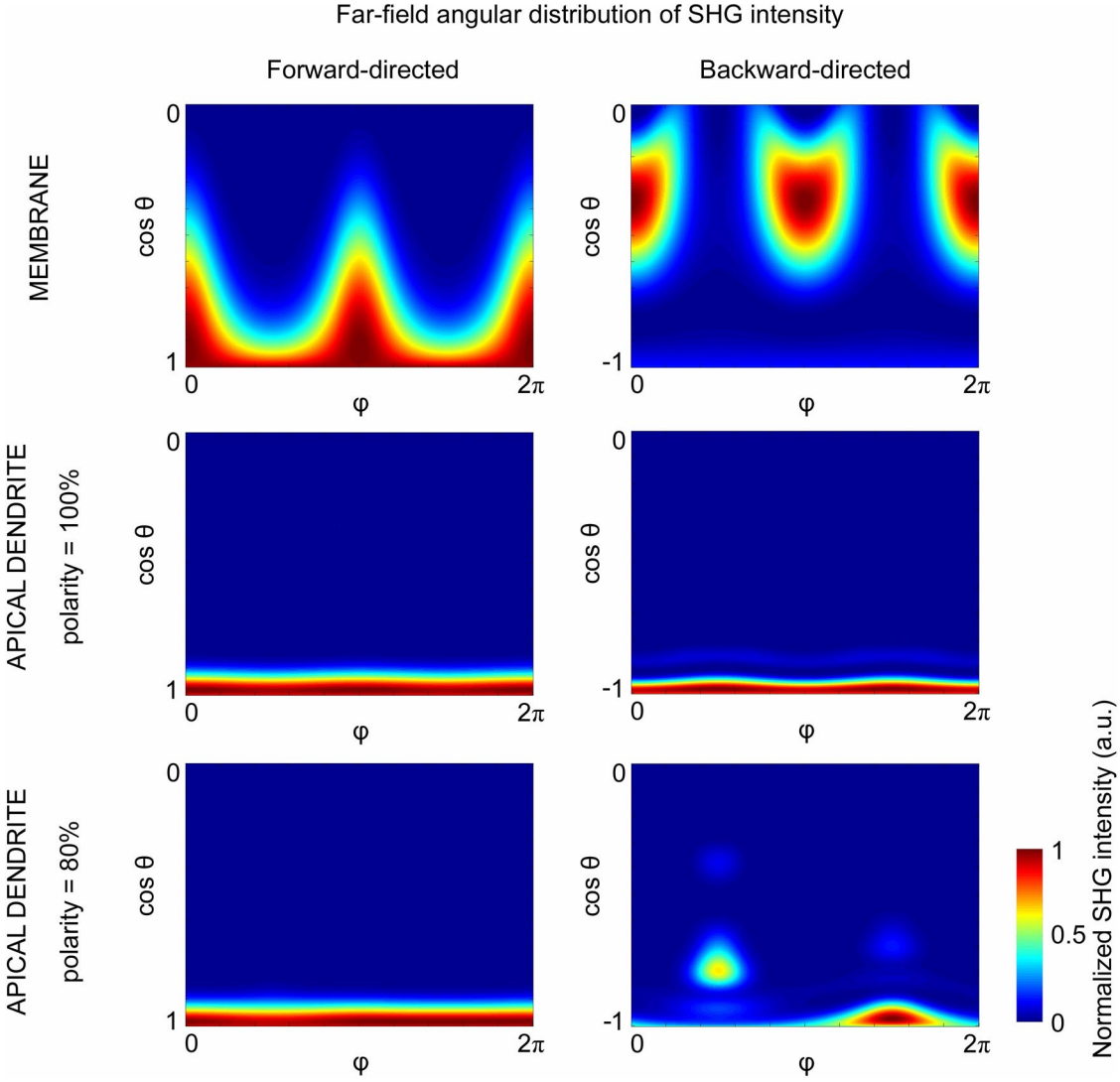

Fig. S2. Simulated far-field angular distribution of SHG intensity for dipoles arranged in two model configurations: a two-dimensional planar array (i.e., ''membrane'') and a three-dimensional cylindrical structure (i.e., ''apical dendrite''). The first configuration, membrane, consists of dipoles in the *x*-*z* plane (coordinate system described in Fig. 4*A*), which point in the *y* direction and are equally spaced 20 nm apart. The second configuration, apical dendrite, is described in detail in *SI Methods* and is the model used to generate Fig. 4 *B* and *C*. For each of the two configurations, the far-field angular distribution is plotted by using axes $\cos\theta$ and φ. These axes are chosen because the product of $\cos\theta$ and φ is a preserved unit of area in spherical coordinates. For the forward-directed distribution of SHG from the membrane, two peaks can be seen at $\theta = 22°$ and $\varphi = 0°$ or 180°. This is in close agreement with $\theta = 28°$ obtained from analytical calculations in ref. 2 in *SI Methods*. The difference can be explained by the different numerical aperture of the excitation objective, 0.7, used in our simulation. For the apical dendrites, most of the forward- and backward-directed SHG intensities are directed along the path of excitation, which implies that practically most of the emitted photons will be collected by the objectives.